Slab Rollback Orogeny Model: A Test of Concept

Luca Dal Zilio[1,2] [ID] **, Edi Kissling[1]** [ID] **, Taras Gerya[1]** [ID] **, and Ylona van Dinther[1,3]** [ID]

[1]Department of Earth Sciences, ETH Zürich, Zürich, Switzerland, [2]Seismological Laboratory, California Institute of Technology, Pasadena, CA, USA, [3]Department of Earth Sciences, Utrecht University, Utrecht, Netherlands

Abstract Buoyancy forces associated with subducting lithosphere control the dynamics of convergent margins. In the postcollisional stage these forces are significantly reduced, yet mountain building and seismicity are ongoing, albeit at lower rates. We leverage advances of a newly developed seismo-thermo-mechanical modeling approach to simulate tectonic and seismicity processes in a self-driven subduction and continental collision setting. We demonstrate that the rearrangement of forces due to slab breakoff, in the postcollisional stage, causes bending and rollback of the residual slab, suction forces, and mantle traction at the base of the upper plate, while stress coupling transfers to the shallow crust. Our results provide an explanation for the postcollisional evolution of the Central Alps, where the so-called *Slab Rollback Orogeny* model explains the slow yet persistent upper plate advance, the height of the mountain range, and a seismicity pattern consistent with the different tectonic regimes throughout the orogen.

Plain Language Summary A long-standing debate in tectonophysics evolves around whether vertical or horizontal forces are the primary drivers of mountain building processes. Here we explore this problem using 2-D numerical models in a generic subduction and continental collision setting. Our results show how the postcollisional evolution of the orogen is controlled by a slow, but persistent, sinking and bending of the postbreakoff residual slab. The resulting seismicity pattern shows a broad pattern of different style of faulting, which are consistent with the local tectonic regimes. We find good correlations between our numerical results and the previously conflicting tectonic observations in the Central Alps and the adjacent foreland basin. Our results thus support the hypothesis that the postbreakoff remaining slab exerts a first-order control on the motions and deformations of collisional orogens.

1. Introduction

The process of continent-continent collision in shaping mountain ranges and adjacent foreland basins have intrigued geoscientists for decades (e.g., Beaumont et al., 1996; Forsyth & Uyeda, 1975; Malinverno & Ryan, 1986; Uyeda & Kanamori, 1979; Whipple & Meade, 2006). According to the most commonly used conceptual models, the evolution of mountain belts is largely driven by the horizontal convergence between the two colliding plates (e.g., Handy et al., 2010; Schmid et al., 1996). This view is based on the perception in which a rigid indenter—frequently exemplified by a bulldozer—in combination with kinematic convergence leads to mountain building processes (e.g., Willett, 2010, for a review). These mechanisms have been invoked to explain the accretion of crustal units from both the upper and lower plates, the building of topography, and the surface denudation of the accreted material (e.g., Beaumont et al., 1996; Whipple, 2009).

Similar kinematic assumptions can potentially be applied to the Central Alps (Figure 1) to investigate crustal accretion and surface erosional processes on both the orogen and the adjacent foreland basins. However, models based on these assumptions are problematic in several aspects, as they underestimate the depth of the crust-mantle boundary (i.e., Moho) beneath the core of the orogen of >50% and overestimate the mean topography elevation when principles of isostatic equilibrium are applied (Kissling, 1993). Further, under these assumptions, the strong negative Bouguer anomalies measured in the Central Alps cannot be explained (Lyon-Caen & Molnar, 1989). The crustal roots in the Central Alps have been seismically determined to be ~60 km thick (Figure 1c), and thus far out of conventional isostatic equilibrium with a mean surface topography of only ~2 km (Kissling, 1993). This evidence leads to the notion that the Alpine roots are overcompensated by many kilometers. How to reconcile this with models of orogenic evolution remains unclear.
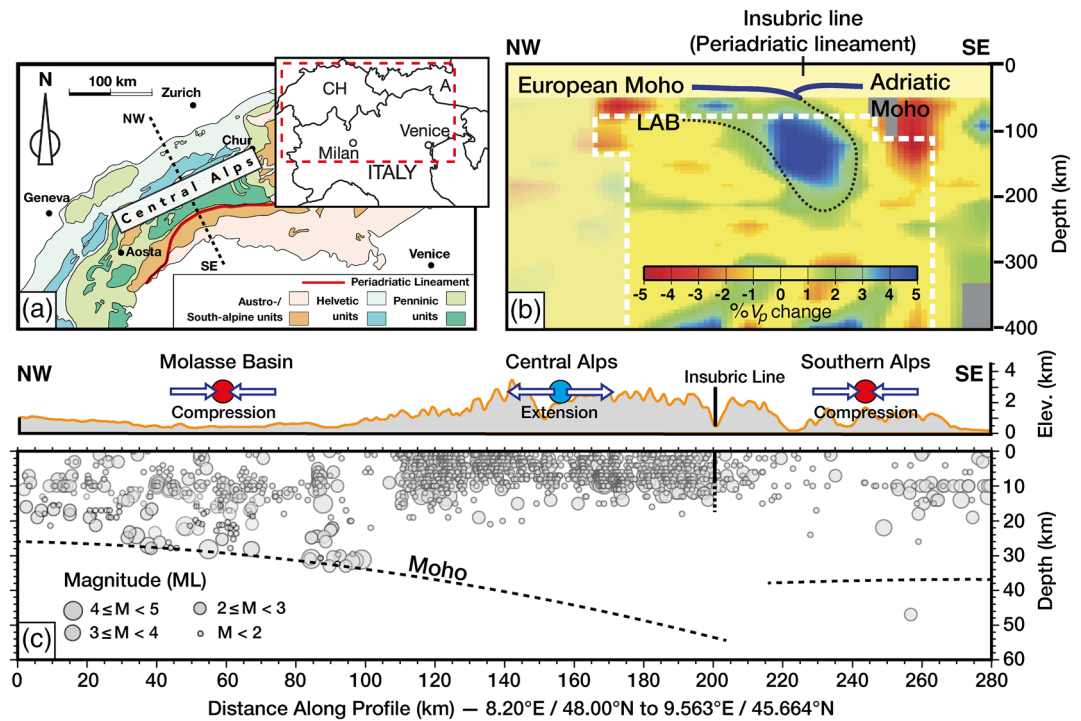
Figure 1. (a) Inset map illustrating the Alps and its foreland basin along with the section discussed in this study. (b) Teleseismic tomography cross section illustrating the geometry of the European slab beneath the central Alps (Lippitsch et al., 2003). White dashed line indicate the region with high resolution. The figure shows lateral variations of *P* wave velocity *Vp* beneath the Moho. (c) Topographic profile and vertical cross section approximately perpendicular to the strike of the Central Alps. Transparent gray circles represent earthquake hypocenters (Singer et al., 2014). Dashed black lines indicate the Moho with a ± 3-km uncertainty of the depth (Spada et al., 2013).

A more recent, alternative explanation suggests that sinking and bending of >180-km-long European lithospheric mantle, in addition to topographic loads, are required to maintain the mountain range close to force equilibrium and to sustain the Alpine topography (Schlunegger & Kissling, 2015). This revised view on the Central Alpine Orogeny, which we refer to as *Slab Rollback Orogeny* (SRO) model (Kissling & Schlunegger, 2018), suggests that the postcollisional evolution of Central Alps evolved in response to a slab rollback process, in which the buoyancy forces of a retreating subduction are driven by the well-known concepts of slab sinking and retreat (Brun & Faccenna, 2008; Malinverno & Ryan, 1986; Royden, 1993), and force balance (Forsyth & Uyeda, 1975). According to the SRO model, slab sinking and bending-related suction forces have been sufficiently strong to drag the overriding Adriatic microplate throughout the long-term subduction and collision, and even during postcollisional convergence (i.e., after slab detachment). Such a rollback mechanism provides a dynamically consistent mechanism to explain the construction of thick sedimentary successions in the Molasse basin where the extra slab load has maintained the Alpine surface at moderate elevations (Schlunegger & Kissling, 2015). Finally, the SRO model provides a viable mechanism to explain the seismicity pattern beneath the Molasse foreland basin, where middle to lower crustal earthquakes (20–30 km deep) are predominantly characterized by bending-related normal-faulting events (Singer et al., 2014) (Figure 1c). This leads to the hypothesis that sinking and bending of the remaining slab have been at work beneath the Central Alps, at least in the last ~20 My.

Thus far, numerical models of subduction have widely been used to study, for example, mantle-lithosphere interactions (e.g., Billen, 2008; Capitanio et al., 2010; Dal Zilio, Faccenda, & Capitanio, 2018), continental collision processes (e.g., Faccenda et al., 2009; Magni et al., 2014; Pusok et al., 2018), surface denudation (e.g., Erdős et al., 2019; Willett, 1999), and slab breakoff (e.g., J. H. Davies & von Blanckenburg, 1995; Duretz et al., 2011; Magni et al., 2013; van Hunen & Allen, 2011). However, less work has been done in studying the postcollisional dynamics. In particular, the open question is whether buoyancy forces and mantle-lithosphere interaction are capable of sustaining the retreat process of a collisional orogen, even after slab breakoff. In this study, we leverage advances of a newly developed, 2-D seismo-thermo-mechanical

(STM) model to simulate both the long-term tectonic and the short-term seismicity of a generic convergent margin, from subduction to collisional orogeny. Our intent here is to investigate the interplay and balance between driving and resisting forces as well as plate motions and crustal deformations. This allows probing how driving and resistive forces control the dynamics, tectonics, and seismicity of a postcollisional margin. Lastly, we discuss possible applications of our model to the Central Alps collision system.

2. Seismo-Thermo-Mechanical (STM) Modeling

We perform simulations using the 2-D, continuum-based, finite difference code STM (van Dinther et al., 2013). This modeling framework utilizes a fully staggered Eulerian grid and freely advecting Lagrangian markers storing the rock properties (Gerya & Yuen, 2003). Conservation of mass, momentum, and heat is implicitly solved for an incompressible medium on the Eulerian grid, whereas physical properties are interpolated to the markers for advection (Gerya & Yuen, 2007). The mechanical equations include inertia and gravity, and the thermal equation includes the effect of radioactive and shear heating, as well as adiabatic heat production/consumption (see the supporting information). Solid-solid phase transformations and density crossover (e.g., eclogitization) are employed via parameterization of phase boundaries using polynomials to interpolate the reaction boundary (Faccenda & Dal Zilio, 2017).

We employ non-Newtonian visco-elasto-plastic rheologies (Gerya & Yuen, 2007). The effective viscosity is calculated from experimentally constrained dislocation creep flow laws (Table S1). The brittle-plastic behavior is taken into account assuming a nonassociative Drucker-Prager yield criterion. Frictional instabilities and healing are introduced by a strongly rate-dependent friction formulation in which the effective friction depends on the slip velocity, which is calculated from the visco-plastic strain rate and effective fault width. When the time step is 1 year, our formulation is reduced to a virtually quasi-dynamic one; however, because of a relatively large smallest time step, our models produce unrealistically long seismic events. Rupture events hence represent the occurrence of rapid slip during which permanent deformation and stress drop occur along a localized plastic shear zone. Nonetheless, other observables, such as slip, surface displacements, rupture widths, and magnitude sizes, agree with natural observations (e.g., Dal Zilio, van Dinther, et al., 2018; van Dinther et al., 2013). The key strength of this invariant formulation allows for spontaneous localization and faulting at any orientation. This means that, instead of being a priori defined, the spontaneous development of faults is governed by local stress and strength states.

The initial model domain consists of two continental plates separated by an oceanic basin (Figures 2a and S1). The dimensions of the computational domain is $3,000 \times 1,200$ km^2 ($1,921 \times 347$ nodes), and all the boundary conditions are free slip. We use a variable grid spacing, which enables to reach a grid resolution of 400 m in the central part of the domain where the continental collision takes place. Subduction initiation is imposed during the early phases of the numerical experiment assuming a 25° dipping weak zone (low plastic strength) on the right ocean-continent transition (Figure 2a). During this period, the oceanic subduction is kinematically prescribed with a fixed convergence rate of 10 cm/year until 200 km of the oceanic slab is subducted into the mantle. After this model initialization step, the convergence rate is removed, and the model is self-driven by internal, buoyancy forces. In this way, the long-term evolution is self-driven and not steady state, as it depends on the slab pull, dissipative forces, and crustal buoyancy. The visco-elasto-plastic thermo-mechanical parameters of each lithology are based on a list of laboratory experiments (Table S1). An extended description of the numerical methodology, model setup, and modeling procedure is given in the supporting information.

3. Results

We present results from the reference model displaying the long-term subduction, collision, and oceanic slab breakoff. We examine how sinking and flexural bending of the remaining slab controls the postcollisional tectonic evolution of the orogen. We then simulate the short-term seismicity pattern and compare it with that of the Central Alps. This comparison allows us to better understand how long-term dynamics relates to the present-day seismicity and crustal tectonics in the Central Alps. Lastly, we explore the sensitivity of our results by varying the age of the oceanic plate (Table S2), which in turn affects its temperature, density contrast (negative buoyancy), and strength (see the supporting information).
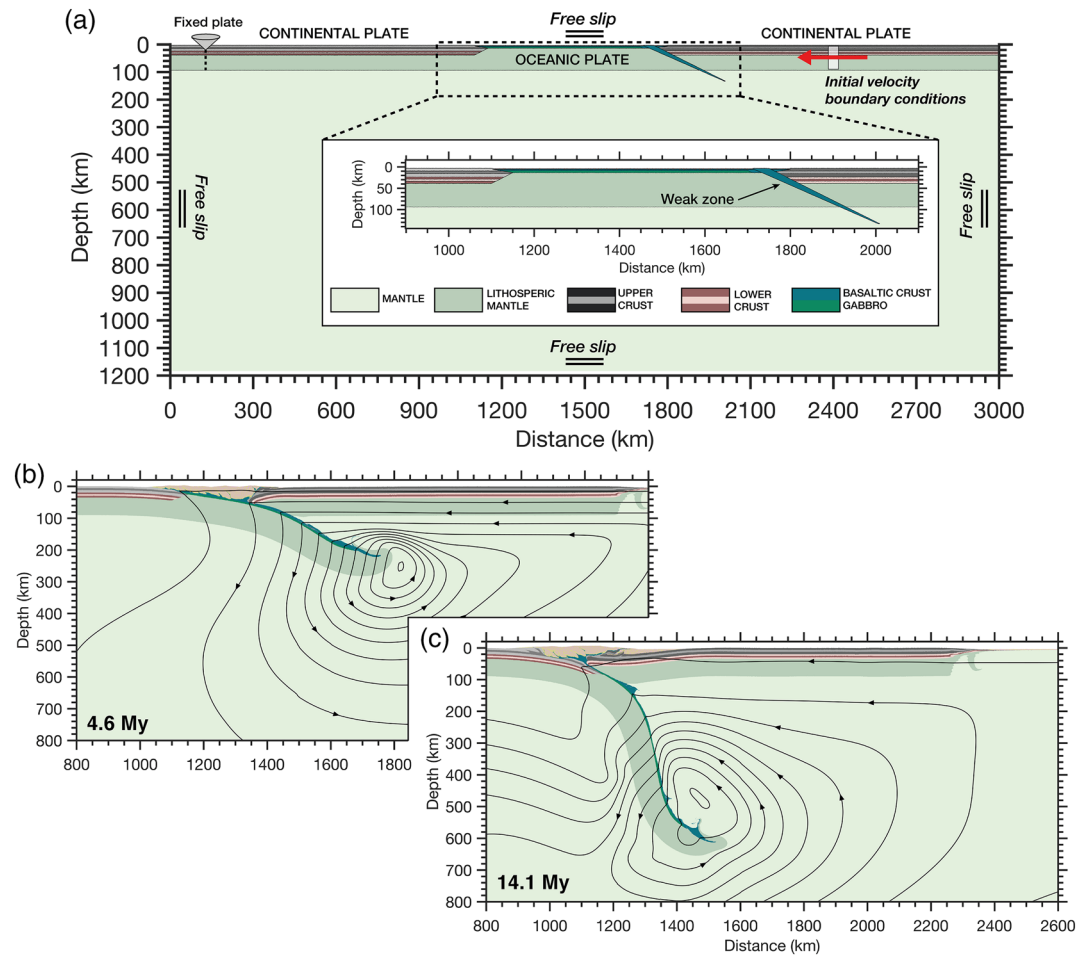
Figure 2. (a) Two-dimensional initial setup. Initial composition map including boundary conditions. The model simulates subduction initiation through the use of a fixed convergence rate (red arrow) on the upper plate until ~200 km of oceanic crust has been subducted. Zoom shows the oceanic plate and preimposed weak zone to initiate subduction. (b, c) Dynamic evolution of a spontaneously retreating subducting plate and mantle-lithosphere interaction after 4.6 and 14.1 My. The superimposed stream function contours display the effect of subduction-induced trench suction and return flow in mantle, which maintain the upper plate coupled with the retreating slab.

3.1. Stage 1: Subduction, Collision, and slab Breakoff

After an initial stage of kinematically imposed subduction initiation, oceanic lithosphere sinks spontaneously at the ocean-upper plate continental margin. Self-sustaining retreating subduction causes the migration of the trench and exerts a suction force to the upper continental plate, while the subduction-induced mantle flow maintains the upper plate highly coupled with the retreating slab (Figures 2b and 2c). Toward the onset of continental collision and indentation, sediments are accreted in the orogenic prism, while the upper plate acts as a buttress. The buoyancy of the continental crust slows down subduction and, hence, the convergence, though a nonnegligible part of continental lithosphere is still being subducted. The collisional zone thus achieves an asymmetric architecture with a doubly vergent thrusting pattern. Slab necking occurs at a relatively shallow depth of approximately 240 km during the stage of slab steepening (Figure S2). Breakoff occurs at the ocean-continent transition a few million years after the collision stage initiated. Slab breakoff and subsequent rebound produce a sharp topographic signal, which results in an uplift rate of ~0.5 mm/year due to a rebound of ~1 km in ~2 My. Such uplift is modulated by the rate of removal of overburden by erosional processes. A simulation example is shown in Movie S1.

3.2. Stage 2: Postcollisional Slab Rollback Evolution of the Orogen

Our numerical experiments indicate that slab detachment is responsible for a stress redistribution within the subducting lithosphere and throughout the orogen. Partial loss of slab pull is followed by a transient
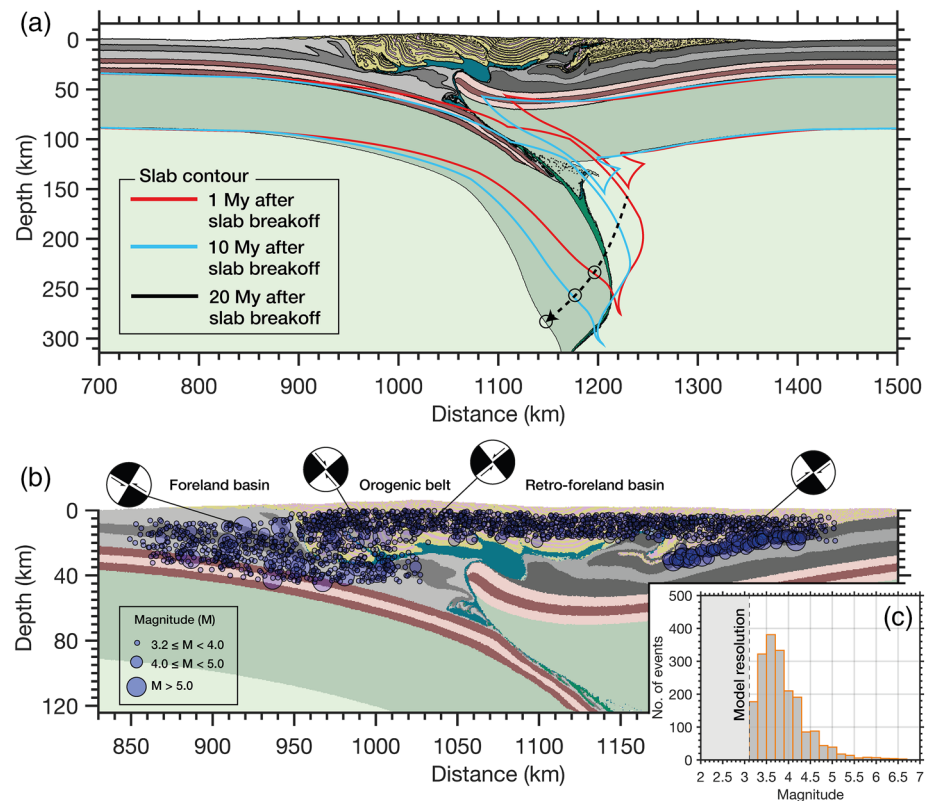
Figure 3. (a) Postcollisional evolution with superimposed contours of the slab geometries at 1 and 10 My after slab breakoff. Compositional map shows the final structure 20 My after slab breakoff. Evolution of the orogen is driven by slow slab rollback and delamination of crustal material. (b) Short-term seismicity pattern of the reference model. Cluster of seismicity and the inferred 2-D focal mechanisms display a broad pattern of different style of faulting, which are consistent with the local tectonic regime. (c) Histograms of all events and the corresponding magnitude.

(<2-My-long) elastic unbending of the remaining slab and an isostatic rebound of the orogenic wedge (Figures S3–S5 and Movie S1). After this transient period, our numerical simulations show that the negative buoyancy—offered by the remaining slab—remains the dominant driving force in the collisional system (Figure 3a), although at lower sinking rates. Slow yet persistent sinking and bending of the remaining slab result in the migration of the whole orogen toward the foreland basin (Figures S3–S5). The ongoing rollback is accompanied by crustal shortening and stacking, which cause shortening on the frontal part of the orogen and in the foreland basin. At deeper crustal levels, buoyant crustal materials are delaminated, while the lower crust continues to subduct at a low, but detectable, sinking rate (Figures 3a and S3). In addition, heat diffusion decreases the flexural strength of the lower plate. This thermo-mechanical process increases the curvature of the lower plate in the asthenosphere, and thus closer to a thermoelastic relaxation of a continental plate to applied loads.

3.3. Stage 3: Regional Stresses and Seismicity Distribution

Results from the seismic cycle simulations show a wide domain subjected to brittle faulting. Seismogenic deformation in the orogenic wedge is largely driven by extensional stresses resulting from the development of retreating subduction (Figures 3b and S3–S5). Because of the yielding of the upper plate, the orogenic wedge partially overthrusts the retro-foreland domain. High compressional stresses are transferred on the upper plate, thus causing a development of a sequence of seismogenic thrusts at the front and beneath the retro-foreland basin (Figure 3b). Deep earthquakes beneath the foreland basin extend into the lower crust, and their distribution correlates well with the flexural bending of the gently to steeply dipping downgoing plate. Flexural bending thus transfers stresses into the lithosphere beneath the foreland basin. Consequently, tectonic stress transfer in the lower and upper crust beneath the foreland results in compressional stresses in the shallower domains and an extensional domain at deeper crustal levels (Figure S6). The laterally variable rheological contrasts between the deeper crustal roots and the brittle shallow crust explain the depth

dependency of the seismicity pattern. Lastly, these results illustrate how the long-term tectonic evolution and crustal properties affect the architecture of the orogen and thereby their short-term spatial distribution of seismicity.

4. Discussion

4.1. SRO Model: Driving and Resistive Forces

The dynamic behavior of subduction systems is governed by the force balance between stresses induced by the buoyancy of the slab and by the viscous flow of the surrounding mantle (G. F. Davies, 1977; McKenzie, 1969; Stevenson & Turner, 1977; Turcotte & Oxburgh, 1967). Our results show that such dynamic behavior holds even during the syncollisional and postcollisional phases, although at very reduces rates. Despite partial loss of the negative buoyancy due to slab breakoff, the postcollisional sinking and flexural bending of the remaining slab are still capable of sustaining slab retreat and suction of the upper plate (Figure 3a).

In our numerical experiments, the main driving force responsible for the motion of tectonic plates is the slab sinking force (i.e., negative buoyancy), which is defined as

$$F_s = \int \int_A \bar{\rho}_m(z) - \bar{\rho}_s(z) \, g \ dx \, dz, \tag{1}$$

where $\bar{\rho}_m$ and $\bar{\rho}_s$ stand for the mean mantle and slab density at a given depth (z), respectively, whereas g is the acceleration of gravity and A the 2-D area of the slab. After detachment, the reduced slab area yields to an F_s of $\sim$8–9 $\cdot$ 10^{12} N/m. In response to slab sinking, poloidal mantle flow is induced in front of the slab tip, which in turn generates basal shear stresses beneath the overriding plate (Figures 4a and 4b). Notably, our models show that shear stresses localize at a characteristic length ($L_c \approx 180$ km; Figure 4d), which corresponds to the effective length of the remaining slab. We then compute the magnitude and time evolution of mantle flow traction force by integrating shear stresses at the base of the overriding plate (Figure 4e):

$$F_t = \int_{L_{up}} \sigma_{xy} \, dx, \tag{2}$$

where L_{up} is the length of the upper plate, whereas shear stresses are proportional to the upper mantle viscosity and the vertical gradient of the horizontal velocity. After slab detachment, basal traction beneath the upper plate initially grows over time (Figure 4e); however, when the slab becomes (sub)vertical and the bending moment is released, the sinking rate slows down. As a result, the response of mantle flow and the basal traction beneath the upper plate diminish.

Our results indicate that, when the underlying continental crust is dragged into the mantle to depths of $\sim$110–120 km, large buoyancy forces are generated, and slab sinking slows down. These deep crustal domains are then warmed up, delaminated, and extruded (Movie S1). According to our results, the forward migration of the mountain range toward the foreland basin, coeval with crustal deformation—ductile at depth and brittle at shallower levels—is governed by a combined effect of slab sinking and bending, and buoyancy forces of the crustal root. More importantly, these processes create a positive feedback as delaminated material from the lower plate increases the relative importance of the vertical slab load, thus promoting further down warping of the plate. Also, this mechanism localizes extensional stresses both at the Moho and within the lower crust (Figures 4c and S6), with the consequence of intracrustal seismicity at both shallow and deep crustal levels (Figure 3b).

The mantle-lithosphere interaction observed in our models emerges naturally and explains why the upper and lower continental plates are mechanically coupled even in the absence of any preimposed convergence rate (Figures 4a, 4b, and S3). Extensional and compressive stresses coexist across the orogen and at different depth levels (Figure 4f). Within the lithospheric mantle, horizontal stresses propagate from the lower plate to the upper plate. The lower plate is subjected to an in-plane force and a bending moment, which depend on the magnitude of the slab sinking force. The resulting lithospheric flexure leads to extensional stresses within the bending region, while large suction forces propagate across the plate interface triggering compressional stress within the lower plate (Figure 4c). At shallower crustal levels, horizontal stresses are generally lower. Notably, the underlying dynamics results in a compression-extension-compression regime. Intraorogenic extension is ascribed to a combination of buoyancy-driven extrusion of the crustal roots and
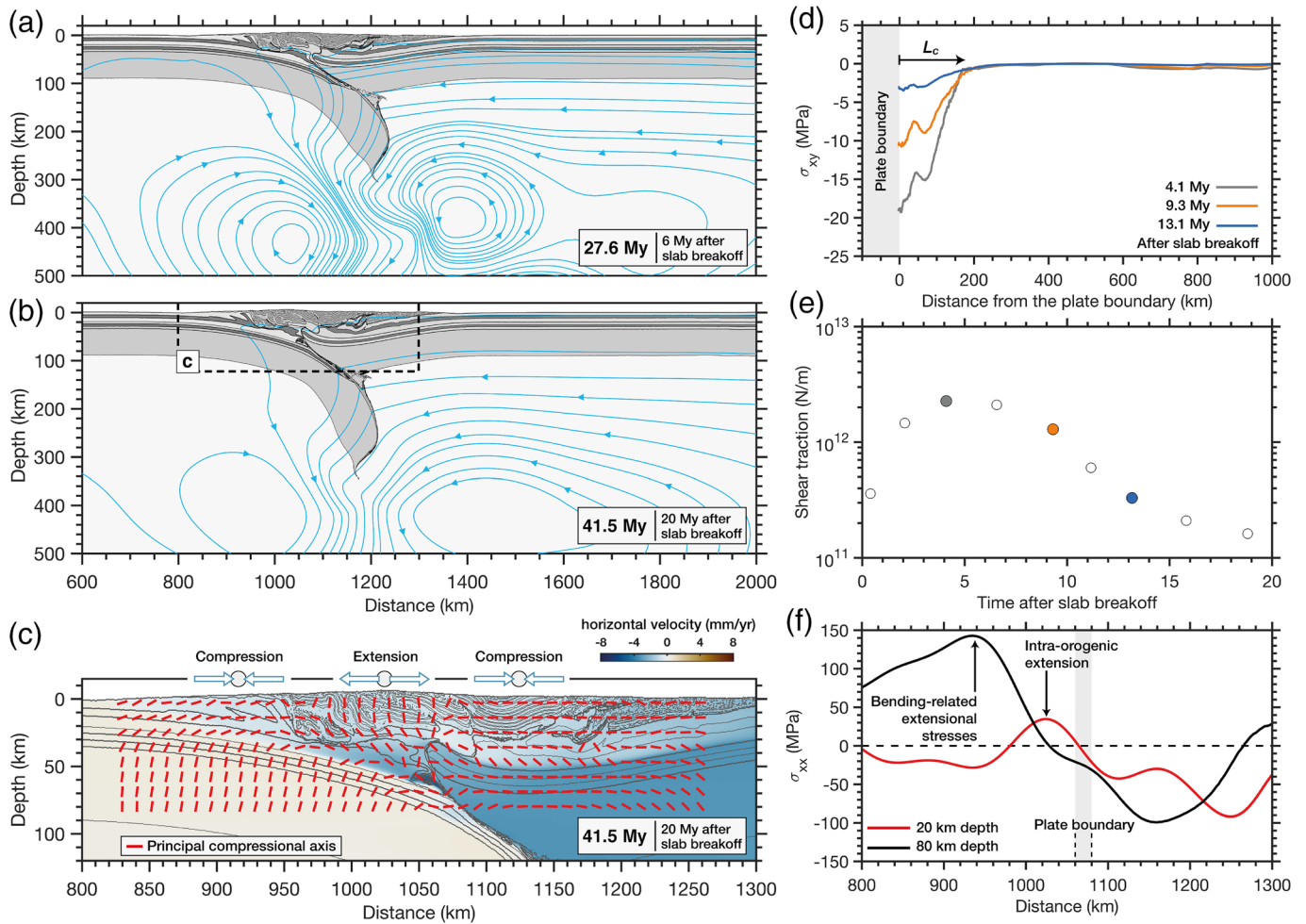
Figure 4. (a, b) Key stages of mantle lithosphere 27.6 and 41.5 My after slab breakoff. Rock composition (gray-scale map) and contour of stream function in light-blue display sinking and retreat of the remaining slab, which cause poloidal mantle flow and basal shear stresses beneath the upper plate. (c) Zoom of the spatial distribution of horizontal velocity. Red bars indicate orientation of maximum (compression) principal stresses. The inferred stress axes show a broad pattern of different tectonic regimes throughout the orogen (compression-extension-compression), which are consistent with the style of faulting and seismicity pattern. (d) Profiles of basal shear stress for different postcollisional stages of the reference model. (e) Time evolution of shear traction at the base of the upper plate. Gray, orange, and blue markers correspond to the profile shown in panel (d). (f) Profiles of horizontal stress throughout the orogen at 20- and 80-km depth (time: 41.5–20 My after slab breakoff). Positive is extension; negative is compression.

gravitational potential energy governed by the topographic and crustal thickness variation between the mountain range and hinterland. As a result, compressional stresses are transmitted on both the pro-foreland and retro-foreland basins.

Note that the SRO model develops for certain age of the oceanic plate (Table S2). The age of the downgoing slab has a first-order effect on the temperature structure, density contrast (i.e., negative buoyancy), and stiffness of the lithosphere. By varying the plate's age, we find that the older the plate, the deeper the slab breakoff (Figures S7–S14). In particular, the age-dependent sinking of the remaining slab depends on its postbreakoff length, as it modulates the sinking force and, in turn, the characteristic length (L_c) and magnitude of mantle flow traction at the base of the upper plate. On the one hand, when slab breakoff is shallow (Figures S8–S10), the postcollisional dynamics are negligible, and the seismicity is entirely restricted to a few events within the orogen (Figure S15a). On the other hand, when the SRO model emerges (Figures 3 and S15b), the seismicity pattern predicts a distribution of earthquakes similar to that observed in the Central Alps (Figure 1c). In our models, the postcollisional retreat of the remaining slab and buoyancy forces control the dynamic coupling and tectonic stress transfer between the upper and lower plates and within

the orogen. Such a stress transfer leads to seismic events with a compressional component beneath the foreland basin and in the upper plate, and with an extensional component in the lower crust and in the core of the orogen.

4.2. SRO Model for the Tectonic Evolution of the Central Alps

A first-order comparison between our results and the Central Alps (Figure 1) shows some interesting similarities at the scale of the orogen. The dynamic evolution of our model is consistent with palaeomagnetic evidence that the lower (European) continental plate has remained nearly stationary since the Late Cretaceous (Dewey et al., 1989), while the upper continental plate was decoupled from Africa and converging against Europe (Platt et al., 1989). This means that the subduction of the Alpine Tethys occurred through a rollback process, and it continued through the syncollisional and postcollisional phases (Froitzheim et al., 1997). Teleseismic tomography cross sections have shown that, along the NW-SE transect across the Central Alps (Figure 1b), the slab dips with only ~60° (Kästle et al., 2019; Lippitsch et al., 2003), suggesting that the remaining slab beneath the Central Alps might still be subjected to a bending moment and an axial force. Seismic anisotropy studies suggest that imbricate stack of lower crustal material—delaminated from the European crust—is consistent with a rollback process (Fry et al., 2010). Notably, our reference model reproduces an isostatic balance between the ~60-km-thick buoyant crustal roots and the negative buoyancy provided by the remaining slab, which modulates the sinking rate and the relatively low orogen topography. The orogen, like for the Central Alps, sits mostly on the lower continental plate, with a topography that does not exceed 5 km in height. The postcollisional convergence rate is relatively small (2–3 mm/year; Figure 4c), and in agreement with GPS measurements (Calais et al., 2002). Finally, from 10 to 20 My after slab breakoff, crustal shortening propagates toward the foreland basin, similarly to the shallow crustal shortening observed in the Jura thrust belt over the last 10 Ma (e.g., Burkhard, 1990).

In terms of the detailed architecture of the orogen, the presented modeling results are largely simplified compared to the much more complicated Alpine system. Our model does not include three-dimensional effects of a collisional margin (e.g., Magni et al., 2017; Pusok et al., 2018), including the interaction between subducting slabs (e.g., Király et al., 2016) and magmatism (e.g., Menant et al., 2016). Also, even excluding along-strike variations of the Alpine arc, details of each individual tectonic structure cannot be expected to be reproduced in a self-driven, generic model such as the ones of this study. On the other hand, the advantage of this model setup is the possibility of simulating a generic convergent margin and analyzing the driving forces and seismic behavior acting on the system.

5. Conclusions

This work focuses on the postcollisional evolution of orogens. Our results show the terminal stage of collision and slab breakoff demonstrating that, although driving forces are significantly reduced, the negative buoyancy offered by the remaining slab is sufficient to control the evolution of postcollisional orogens. Sinking and bending of the remaining slab cause suction forces toward the plate boundary and mantle tractions force at the base of the upper plate. The thermal age of the detached oceanic plate is crucial for the occurrence of the SRO process, as it controls the mantle flow through density contrast (negative buoyancy) and depth of slab breakoff, setting the characteristic distance under which basal shear stresses localize. Competition between the negative buoyancy of the remaining slab and thick buoyant crustal roots modulates slab sinking, thus maintaining the orogens' topography relatively low.

This so-called SRO model offers an explanation for the ensemble of observations extracted from the Central Alps (Kissling & Schlunegger, 2018), including (1) the stacking of nappes (Fry et al., 2010), (2) the force balance with the thick and buoyant crustal root, (3) the postcollisional evolution of the Molasse foreland basin (Schlunegger & Kissling, 2015), and (4) the current seismicity pattern in the Central Alps (Singer et al., 2014). Notably, slab retreat and upper mantle confined dynamics are features commonly found in other postcollisional convergent margins, including the Apennines (e.g., Carminati et al., 2003; D'Acquisto et al., 2020) and in most of the circum-Mediterranean arc (Brun & Faccenna, 2008; Faccenna et al., 2004; Jolivet et al., 2013; Royden, 1993). In light of these results, while the evolution of the Himalayas serves as a much better example where mountain building processes and collision are ongoing, the understanding of the recent geologic history of the Central Alps requires an alternative view.

Data Availability Statement

Figures were made using perceptually uniform colormaps (Crameri, 2018). Data related to this study can be downloaded online (from https://doi.org/10.22002/D1.1376).

References

Beaumont, C., Ellis, S., Hamilton, J., & Fullsack, P. (1996). Mechanical model for subduction-collision tectonics of alpine-type compressional orogens. *Geology*, *24*(8), 675–678.

Billen, M. I. (2008). Modeling the dynamics of subducting slabs. *Annual Review of Earth and Planetary Sciences*, *36*, 325–356.

Brun, J.-P., & Faccenna, C. (2008). Exhumation of high-pressure rocks driven by slab rollback. *Earth and Planetary Science Letters*, *272*(1-2), 1–7.

Burkhard, M. (1990). Aspects of the large-scale miocene deformation in the most external part of the Swiss Alps (sub-Alpine Molasse to Jura Fold Belt). *Eclogae Geologicae Helvetiae*, *83*(3), 559–583.

Calais, E., Nocquet, J.-M., Jouanne, F., & Tardy, M. (2002). Current strain regime in the Western Alps from continuous global positioning system measurements, 1996–2001. *Geology*, *30*(7), 651–654.

Capitanio, F. A., Stegman, D. R., Moresi, L.-N., & Sharples, W. (2010). Upper plate controls on deep subduction, trench migrations and deformations at convergent margins. *Tectonophysics*, *483*(1), 80–92.

Carminati, E., Doglioni, C., & Scrocca, D. (2003). Apennines subduction-related subsidence of Venice (Italy). *Geophysical Research Letters*, *30*(13), 1717 en. https://doi.org/10.1029/2003GL017001

Crameri, F. (2018). Geodynamic diagnostics, scientific visualisation and StagLab 3.0. *Geoscientific Model Development*, *11*(6), 2541–2562.

D'Acquisto, M., Dal Zilio, L., Molinari, I., Kissling, E., Gerya, T., & van Dinther, Y. (2020). Tectonics and seismicity in the northern Apennines driven by slab retreat and lithospheric delamination. *Tectonophysics*, *789*, 228,481.

Dal Zilio, L., Faccenda, M., & Capitanio, F. (2018). The role of deep subduction in supercontinent breakup. *Tectonophysics*, *746*, 312–324.

Dal Zilio, L., van Dinther, Y., Gerya, T. V., & Pranger, C. C. (2018). Seismic behaviour of mountain belts controlled by plate convergence rate. *Earth and Planetary Science Letters*, *482*, 81–92.

Davies, G. F. (1977). Viscous mantle flow under moving lithospheric plates and under subduction zones. *Geophysical Journal International*, *49*(3), 557–563.

Davies, J. H., & von Blanckenburg, F. (1995). Slab breakoff: A model of lithosphere detachment and its test in the magmatism and deformation of collisional orogens. *Earth and Planetary Science Letters*, *129*(1-4), 85–102.

Dewey, J. F., Helman, M. L., Knott, S. D., Turco, E., & Hutton, D. H. W. (1989). Kinematics of the western mediterranean. *Geological Society, London, Special Publications*, *45*(1), 265–283.

Duretz, T., Gerya, T. V., & May, D. A. (2011). Numerical modelling of spontaneous slab breakoff and subsequent topographic response. *Tectonophysics*, *502*(1-2), 244–256.

Erdős, Z., Huismans, R. S., & Beek, P. (2019). Control of increased sedimentation on orogenic fold-and-thrust belt structure—Insights into the evolution of the Western Alps. *Solid Earth*, *10*(2), 391–404.

Faccenda, M., & Dal Zilio, L. (2017). The role of solid-solid phase transitions in mantle convection. *Lithos*, *268*, 198–224.

Faccenda, M., Minelli, G., & Gerya, T. V. (2009). Coupled and decoupled regimes of continental collision: Numerical modeling. *Earth and Planetary Science Letters*, *278*(3-4), 337–349.

Faccenna, C., Piromallo, C., Crespo-Blanc, A., Jolivet, L., & Rossetti, F. (2004). Lateral slab deformation and the origin of the western Mediterranean arcs. *Tectonics*, *23*(1), TC1012. https://doi.org/10.1029/2002TC001488

Forsyth, D., & Uyeda, S. (1975). On the relative importance of the driving forces of plate motion. *Geophysical Journal International*, *43*(1), 163–200.

Froitzheim, N., Conti, P., & Van Daalen, M. (1997). Late cretaceous, synorogenic, low-angle normal faulting along the Schlinig fault (Switzerland, Italy, Austria) and its significance for the tectonics of the Eastern Alps. *Tectonophysics*, *280*(3-4), 267–293.

Fry, B., Deschamps, F., Kissling, E., Stehly, L., & Giardini, D. (2010). Layered azimuthal anisotropy of Rayleigh wave phase velocities in the European alpine lithosphere inferred from ambient noise. *Earth and Planetary Science Letters*, *297*(1-2), 95–102.

Gerya, T. V., & Yuen, D. A. (2003). Characteristics-based marker-in-cell method with conservative finite-differences schemes for modeling geological flows with strongly variable transport properties. *Physics of the Earth and Planetary Interiors*, *140*(4), 293–318.

Gerya, T., & Yuen, D. (2007). Robust characteristics method for modelling multiphase visco-elasto-plastic thermo-mechanical problems. *Physics of the Earth and Planetary Interiors*, *163*(1), 83–105.

Handy, M. R., Schmid, S. M., Bousquet, R., Kissling, E., & Bernoulli, D. (2010). Reconciling plate-tectonic reconstructions of Alpine Tethys with the geological-geophysical record of spreading and subduction in the Alps. *Earth-Science Reviews*, *102*(3-4), 121–158.

Jolivet, L., Faccenna, C., Huet, B., Labrousse, L., Le Pourhiet, L., Lacombe, O., et al. (2013). Aegean tectonics: Strain localisation, slab tearing and trench retreat. *Tectonophysics*, *597*, 1–33.

Kästle, E. D., Rosenberg, C., Boschi, L., Bellahsen, N., Meier, T., & El-Sharkawy, A. (2019). Slab break-offs in the Alpine Subduction Zone. *Solid Earth Discussions*, *2019*, 1–16.

Király, A., Capitanio, F. A., Funiciello, F., & Faccenna, C. (2016). Subduction zone interaction: Controls on arcuate belts. *Geology*, *44*(9), 715–718.

Kissling, E. (1993). Deep structure of the alps—What do we really know? *Physics of the Earth and Planetary Interiors*, *79*(1-2), 87–112.

Kissling, E., & Schlunegger, F. (2018). Rollback orogeny model for the evolution of the Swiss Alps. *Tectonics*, *37*(4), 1097–1115. https://doi.org/10.1002/2017TC004762

Lippitsch, R., Kissling, E., & Ansorge, J. (2003). Upper mantle structure beneath the Alpine Orogen from high-resolution teleseismic tomography. *Journal of Geophysical Research*, *108*(B8), 2376. https://doi.org/10.1029/2002JB002016

Lyon-Caen, H., & Molnar, P. (1989). Constraints on the deep structure and dynamic processes beneath the alps and adjacent regions from an analysis of gravity anomalies. *Geophysical Journal International*, *99*(1), 19–32.

Magni, V., Allen, M. B., van Hunen, J., & Bouilhol, P. (2017). Continental underplating after slab break-off. *Earth and Planetary Science Letters*, *474*, 59–67.

Magni, V., Faccenna, C., van Hunen, J., & Funiciello, F. (2013). Delamination vs. break-off: The fate of continental collision. *Geophysical Research Letters*, *40*, 285–289. https://doi.org/10.1002/grl.50090

Magni, V., Faccenna, C., van Hunen, J., & Funiciello, F. (2014). How collision triggers backarc extension: Insight into Mediterranean style of extension from 3-D numerical models. *Geology*, *42*(6), 511–514.

Malinverno, A., & Ryan, W. B. F. (1986). Extension in the Tyrrhenian Sea and shortening in the Apennines as result of arc migration driven by sinking of the lithosphere. *Tectonics*, *5*(2), 227–245.

McKenzie, D. P. (1969). Speculations on the consequences and causes of plate motions. *Geophysical Journal International*, *18*(1), 1–32.

Menant, A., Sternai, P., Jolivet, L., Guillou-Frottier, L., & Gerya, T. (2016). 3D numerical modeling of mantle flow, crustal dynamics and magma genesis associated with slab roll-back and tearing: The Eastern MXediterranean case. *Earth and Planetary Science Letters*, *442*, 93–107.

Platt, J. P., Behrmann, J. H., Cunningham, P. C., Dewey, J. F., Helman, M., Parish, M., et al. (1989). Kinematics of the alpine arc and the motion history of adria. *Nature*, *337*(6203), 158.

Pusok, A. E., Kaus, B. J. P., & Popov, A. A. (2018). The effect of rheological approximations in 3-D numerical simulations of subduction and collision. *Tectonophysics*, *746*, 296–311.

Royden, L. H. (1993). The tectonic expression slab pull at continental convergent boundaries. *Tectonics*, *12*(2), 303–325.

Schlunegger, F., & Kissling, E. (2015). Slab Rollback Orogeny in the Alps and evolution of the Swiss Molasse Basin. *Nature communications*, *6*.

Schmid, S. M., Pfiffner, O. A., Froitzheim, N., Schönborn, G., & Kissling, E. (1996). Geophysical-geological transect and tectonic evolution of the Swiss-Italian alps. *Tectonics*, *15*(5), 1036–1064.

Singer, J., Diehl, T., Husen, S., Kissling, E., & Duretz, T. (2014). Alpine lithosphere slab rollback causing lower crustal seismicity in northern foreland. *Earth and Planetary Science Letters*, *397*, 42–56.

Spada, M., Bianchi, I., Kissling, E., Agostinetti, N. P., & Wiemer, S. (2013). Combining controlled-source seismology and receiver function information to derive 3-D moho topography for Italy. *Geophysical Journal International*, *194*(2), 1050–1068. https://doi.org/10.1093/gji/ggt148

Stevenson, D. J., & Turner, J. S. (1977). Angle of subduction. *Nature*, *270*(5635), 334–336.

Turcotte, D. L., & Oxburgh, E. R. (1967). Finite amplitude convective cells and continental drift. *Journal of Fluid Mechanics*, *28*(01), 29–42.

Uyeda, S., & Kanamori, H. (1979). Back-arc opening and the mode of subduction. *Journal of Geophysical Research*, *84*(B3), 1049–1061.

van Dinther, Y., Gerya, T. V., Dalguer, L. A., Mai, P. M., Morra, G., & Giardini, D. (2013). The seismic cycle at subduction thrusts: Insights from seismo-thermo-mechanical models. *Journal of Geophysical Research: Solid Earth*, *118*, 6183–6202. https://doi.org/10.1002/2013JB010380

van Hunen, J., & Allen, M. B. (2011). Continental collision and slab break-off: A comparison of 3-D numerical models with observations. *Earth and Planetary Science Letters*, *302*(1-2), 27–37.

Whipple, K. X. (2009). The influence of climate on the tectonic evolution of mountain belts. *Nature Geoscience*, *2*(2), 97.

Whipple, K. X., & Meade, B. J. (2006). Orogen response to changes in climatic and tectonic forcing. *Earth and Planetary Science Letters*, *243*(1-2), 218–228.

Willett, S. D. (1999). Orogeny and orography: The effects of erosion on the structure of mountain belts. *Journal of Geophysical Research*, *104*(B12), 28,957–28,981.

Willett, S. D. (2010). Late Neogene erosion of the Alps: A climate driver? *Annual Review of Earth and Planetary Sciences*, *38*, 411–437.